# Nonlinear Competition Avoidance Favors Coexistence in Spatially Structured Microbial Populations

Mattia Mattei,[1] David Soriano-Paños,[1,2] and Alex Arenas[1,3]
[1]*Departament d'Enginyeria Informàtica i Matemàtiques, Universitat Rovira i Virgili, 43007 Tarragona, Spain*
[2]*GOTHAM Laboratory, Institute for Biocomputation and Physics of Complex Systems, University of Zaragoza, 50018 Zaragoza, Spain*
[3]*ComSCIAM, Universitat Rovira i Virgili, 43007 Tarragona, Spain*

(Received 20 January 2026; accepted 30 September 2026; published 5 November 2026)

Bacteria regulate their motility through a variety of mechanisms, including quorum sensing and other density-dependent responses mediated by diffusible signals. While nonlinear density-dependent motility is well known in active-matter theory to generate nonequilibrium spatial patterns, its consequences for the coexistence of growing, interacting species remain less explored. Here we develop a minimal spatially structured model for two strongly competing species in which local demographic interactions are coupled to an escape response: Each species increases its motility nonlinearly (sigmoidal) with the local abundance of its competitor. We show that this sigmoidal motility regulation promotes optimal spatial self-organization and can sustain long term coexistence via segregation, even in parameter regimes that yield competitive exclusion in well-mixed Lotka-Volterra dynamics. On two-dimensional lattices, the interplay between demographic competition and density-dependent motility generates a range of emergent patterns, including regimes in which the weaker competitor counterintuitively has higher total abundance. Overall, our results identify nonlinear, competitor-induced motility as a fundamental mechanism capable of sustaining coexistence in competing microbial populations.

DOI: 10.1103/4t9n-nvgc

## I. INTRODUCTION

Many bacterial species exhibit various forms of motility, ranging from swimming in liquid environments to coordinated swarming across solid substrates [1]. These behaviors are often regulated responses to environmental and physiological signals, mediated by mechanisms such as chemotaxis [2] or quorum sensing (QS) [3], whereby the accumulated autoinducer signals reflect the local bacteria density and trigger coordinated changes in gene expression. In several species, QS represses motion by downregulating the flagellar apparatus or inducing adhesive phenotypes that favor surface attachment and reduced mobility [4,5]. In contrast, signaling can also stimulate motion: QS-controlled synthesis of biosurfactants such as surfactin in *Bacillus subtilis* [6], putisolvins in *Pseudomonas putida* [7], or Acyl-homoserine lactone-mediated responses in *Rhizobium etli* [8] has been shown to promote swarming, surface expansion, and microcolonization dispersal. All these mechanisms correspond to changes in motility driven by the local concentration of signaling molecules, which reflect the density of the nearby cells that synthesize them.

From a theoretical perspective, density-dependent motility has been a central theme in active-matter physics because it can generate spatial structure in the absence of explicit attractive interactions. Tailleur and Cates [9] showed that run-and-tumble particles which reduce their speed in high density regions can spontaneously separate into dense and dilute phases, a phenomenon now referred to as motility-induced phase separation (MIPS) [10]. Subsequent work has extended these ideas to multispecies systems and to more general forms of density-dependent motility, revealing a rich spectrum of nonequilibrium patterns, including clusters, concentric rings, and propagating bands [11–16].

Although density-dependent motility is well established as a pattern formation mechanism, its consequences for survival and coexistence in growing multispecies communities remain comparatively less explored [17]. This gap is notable given the challenge of explaining the high diversity observed in microbial communities [18]. Coexistence among species competing for the same resources typically requires some form of niche differentiation [19], and such differences may arise from an interplay between local competitive dynamics and spatial processes operating at larger scales. Even in spatially homogeneous environments, coexistence can be achieved through competition-colonization trade-offs, in which superior competitors are poorer colonizers of empty space than inferior ones [20]. Spatial segregation maintained by escape or fugitive strategies [21] of the weaker competitor has been repeatedly documented in ecology [22–24].

This raises the question of whether density-dependent motility can itself generate an effective competition-colonization trade-off in microbial systems. Previous studies have combined density-dependent diffusivity with population dynamics, largely emphasizing the resulting spatial patterns. Cates *et al*. [25] investigated this in a single species

*Published by the American Physical Society under the terms of the Creative Commons Attribution 4.0 International license. Further distribution of this work must maintain attribution to the author(s) and the published article's title, journal citation, and DOI.*

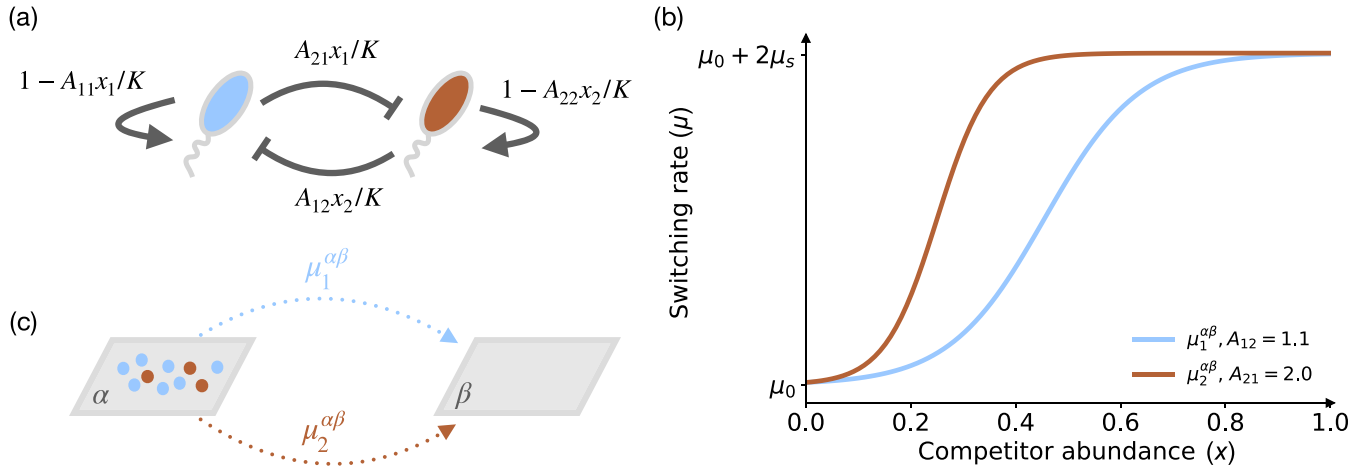



FIG. 1. Schematic illustration of the model. (a) Demographic dynamics within each patch, including intrinsic growth at rate $r$, carrying capacity $K$, and intra- and interspecific competition terms $A_{ii}$ and $A_{ij}$, respectively. (b) Sigmoidal escape response functions [Eq. (2)] for the species 1 with $A_{12} = 1.1$ (blue line) and for species 2 for $A_{21} = 2.0$ (red line), considering $\Delta = 0.5$ and $\xi = 10$. (c) Initial configuration of the system in the case of the two-patches setting, in which both species are initially present in patch $\alpha$ and may subsequently migrate to patch $\beta$ with species-specific migration rates $\mu_1^{\alpha\beta}$ and $\mu_2^{\alpha\beta}$.

undergoing logistic growth, showing that phase separation can still arise, although growth eventually arrests the coarsening. Curatolo *et al.* [11] analyzed density-dependent motility in a pair of competing bacterial strains, reporting demixing and colocalization patterns, yet within a framework where the species are indistinguishable.

Here we focus instead on coexistence between asymmetrically competing species that would undergo competitive exclusion in a well-mixed Lotka-Volterra setting. We develop a minimal description for two strongly competing species in which local demographic interactions are coupled to an escape response: Each species increases its motility nonlinearly with the local abundance of its competitor, with the strength of the response tied to the strength of interspecific competition.

We show that this coupling can promote coexistence across broad parameter regimes. We first characterize a two-patch setting analytically, isolating how the functional form of the motility response controls the emergence of coexistence. Then we extend the analysis to two-dimensional lattices where the same mechanism generates diverse spatial patterns, including regimes in which the weaker competitor occupies a larger spatial region than its stronger rival.

## II. RESULTS

### A. The model

The model is a standard extension of the competitive Lotka-Volterra equations for two species, labeled by indices 1 and 2, to a spatially structured system. The full system consists of $2m$ coupled equations, where $m$ is the total number of spatial units, or patches. For the abundance of species 1 in patch $\alpha$, $x_1^\alpha(t)$, the dynamics reads

$$\frac{dx_1^\alpha(t)}{dt} = r\,x_1^\alpha(t)\left[1 - \frac{A_{11}}{K}\,x_1^\alpha(t) - \frac{A_{12}}{K}\,x_2^\alpha(t)\right] + \sum_\beta \left[\mu_1^{\beta\alpha}(t)\,x_1^\beta(t) - \mu_1^{\alpha\beta}(t)\,x_1^\alpha(t)\right]. \quad (1)$$

The first line represents the demographic dynamics: $r$ is the intrinsic growth rate, $K$ is an *environmental* carrying capacity parameter setting the characteristic population scale of the system, and $A_{11}$ and $A_{12}$ quantify intraspecific limitation and interspecific competition, respectively. The effective carrying capacity of species $i$ in the absence of competitors is given by $K/A_{ii}$. Furthermore, in our notation, $A_{ij}$ denotes the effect of species $j$ on species $i$. This is schematically represented in Fig. 1(a).

The second line encodes motility between neighboring patches, being $\mu_1^{\alpha\beta}(t)$ the rate at which species 1 move from $\alpha$ to $\beta$ at time $t$. This rate reads:

$$\mu_1^{\alpha\beta}(t) = M_{\alpha\beta}\left[\mu_0 + \frac{2\,\mu_S}{1 + \exp\left[\xi(\Delta - A_{12}\,x_2^\alpha(t)/K)\right]}\right], \quad (2)$$

where we have expressed species motility as the combination of a constant diffusivity $\mu_0$ and a nonlinear sigmoidal modulation that increases with the local abundance of the competitor. The rate parameter $\mu_S$ sets the amplitude of this density-dependent contribution to motility. The choice of a sigmoid function is common when modeling processes such as quorum sensing [11,15,16,26] where reaching a critical density threshold triggers a qualitative change. In our case, such response is an "escape" response, moving a species apart from the areas with high local density of its competitor. The parameter $\xi$ controls the steepness of this response, while $\Delta$ sets its inflection point, that can be seen as an activation threshold for $\xi \to \infty$. Note that the abundance of competitors enters the motility function multiplied by the interaction coefficient $A_{12}$. This choice guarantees that the influence of one species on the growth of the other is consistently mirrored in the modulation of its motility, thereby coupling demographic and escape pressures. This functional form of the escape response is plotted in Fig. 1(b), where we show how the competition coefficients $A_{21}$ and $A_{12}$ affect the steepness and the inflection point of the sigmoid for both species. Finally, $\mathbf{M}$ is an $m \times m$ symmetric matrix that encodes the spatial adjacency

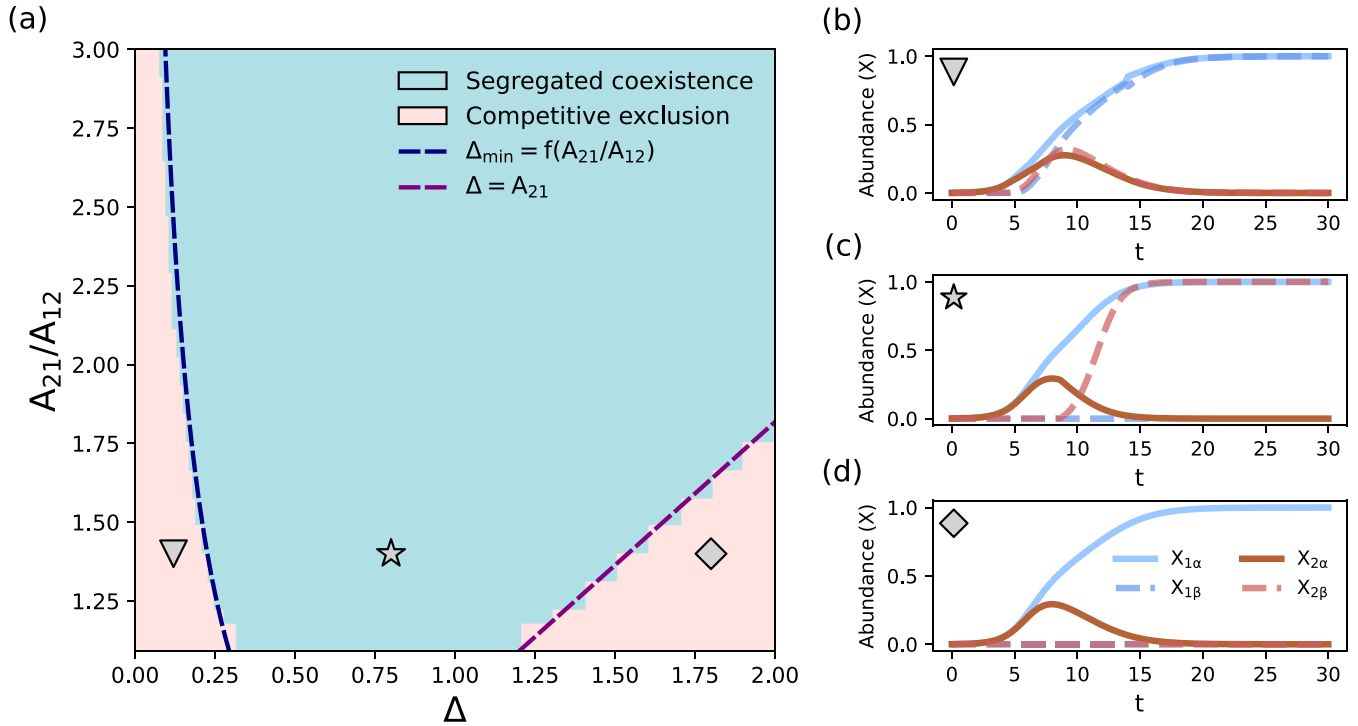



FIG. 2. (a) Phase diagram distinguishing segregated coexistence from competitive exclusion as a function of the motility threshold $\Delta$ and the interaction ratio $A_{21}/A_{12}$ for two neighboring patches, in the theoretical limits $\xi \to \infty$ and $\mu_0 \to 0$. The background heatmap is obtained from numerical integration of Eqs. (1), while dashed lines indicate analytical predictions (see Appendix A). The three markers correspond to the parameter values $A_{21}/A_{12} = 1.4$ and $\Delta = 0.12,\ 0.8,\ 1.8$, for which representative temporal dynamics are shown in panels (b)–(d). [(b)–(d)] Representative time series illustrating the different dynamical outcomes. Symbol ▼ denotes competitive exclusion resulting from the migration of both species to patch $\beta$; ⋆ indicates coexistence driven by the migration of species 2; and ♦ corresponds to competitive exclusion when neither species migrates. All simulations use $A_{11} = A_{22} = 1$, $\mu_S = 0.1$, and $A_{12} = 1.1$.

between patches. In the two-patch scenario, we simply have $M_{\alpha\beta} = M_{\beta\alpha} = 1$. For lattice geometries, neighboring sites satisfy $M_{\alpha\beta} = M_{\beta\alpha} = 1/\mathcal{N}$, where $\mathcal{N}$ denotes the number of nearest neighbors, while all other entries are zero.

In what follows, we work in a fully dimensionless framework. Defining the rescaled variables

$$\tilde{t} \equiv rt, \quad \tilde{x}_i^\alpha \equiv \frac{x_i^\alpha}{K}, \quad \tilde{\mu}_0 \equiv \frac{\mu_0}{r}, \quad \tilde{\mu}_S \equiv \frac{\mu_S}{r},$$

the new dynamics $d\tilde{x}_1^\alpha/d\tilde{t} = 1/(rK) \times dx_1^\alpha/dt$ only involves dimensionless variables and parameters. Throughout the manuscript, species abundances are therefore expressed as fractions of the carrying capacity, while the motility should be interpreted relative to the intrinsic growth rate. For simplicity, we omit the tildes in the following and work exclusively with these rescaled variables. Furthermore, by setting $A_{11} = A_{22} = 1$, we isolate the effects of interspecific competition on both the demographic dynamics and the density-dependent motility.

Throughout, we understand coexistence as long-term persistence of both species at the metapopulation level, i.e., $x_1 = \sum_\alpha x_1^\alpha > 0$ and $x_2 = \sum_\alpha x_2^\alpha > 0$ as $t \to \infty$. In the competitive-exclusion regime $A_{12} > 1$ and $A_{21} > 1$, stable coexistence within a single patch is impossible in the classical Lotka-Volterra dynamics, so coexistence in our spatial system necessarily relies on spatial segregation and/or sustained spatial patterning. In what follows, we begin with the simplified setting consisting of two neighboring patches, and later we extend the analysis to two-dimensional lattices, which can be seen as discrete representations of an underlying continuous space.

### B. Two patches

Let us consider two connected patches, $\alpha$ and $\beta$, and assume an initial condition where a small seed of both species is present only in patch $\alpha$, while patch $\beta$ is empty [Fig. 1(c)]. Regarding the demographic interactions of the species, we assume the regime of competitive exclusion, where, in our setup, the interaction rates must fulfill $A_{12} > 1$, $A_{21} > 1$, and $A_{12} \neq A_{21}$. Within the classical Lotka-Volterra framework, stable coexistence of both species within a single patch is impossible in this regime. Our goal is therefore to investigate whether the nonlinear motility response introduced in Eq. (2) can generate the conditions required for coexistence across the two patches. To address this question, let us first explore the scenario in the limits $\mu_0 \to 0$ and $\xi \to \infty$, thus neglecting the constant bacterial diffusion and considering a step function triggering species motility when the density of the competitor exceeds $\Delta$. We will study later the effects of relaxing both assumptions. Note that in this limit the fully segregated two-patch configuration $(x_1^\alpha, x_1^\beta, x_2^\alpha, x_2^\beta) = (1, 0, 0, 1)$ is an exact asymptotically stable equilibrium.

In Fig. 2(a) we show the phase diagram of the system as a function of the ratio between the interaction rates $A_{21}/A_{12}$

and the motility threshold $\Delta$. The resulting phase diagram reveals a broad coexistence region, which arises specifically from the structure of our motility function. As both species cannot coexist within a single patch, the only viable configuration for both species to thrive is spatial segregation: One species ultimately colonizes one patch while the other species colonizes the other. Under the initial conditions depicted in Fig. 1(c), species 2 must cross its motility activation condition, escape patch $\alpha$ and colonize patch $\beta$, while species 1 must never activate its escape response, preventing it from invading both patches. Mathematically, if $A_{21} > A_{12}$, then this occurs when

$$x_2^{\alpha}(t) < \frac{\Delta}{A_{12}} \quad \forall t \in [0, \infty], \tag{3}$$

so species 1 always stays in $\alpha$ and there exists a time $\tau$ for which

$$x_1^{\alpha}(\tau) \geqslant \frac{\Delta}{A_{21}}, \tag{4}$$

thus triggering the motility of species 2.

For a fixed value of the competition ratio $A_{21}/A_{12}$, increasing the motility threshold $\Delta$ leads to two successive transitions: first from competitive exclusion to coexistence and then from coexistence back to exclusion. The first transition separates a regime in which the dominant species remains mobile and ultimately colonizes both patches, so that condition (3) is violated, from a segregated coexistence state in which each species occupies a different patch and both conditions are satisfied. In Appendix A we analytically derive the boundary between these two regimes, shown as the blue curve in Fig. 2(a). This curve defines the minimum activation threshold, $\Delta_{\min} = f(A_{21}/A_{12})$, required for condition (3) to hold. In Figs. 2(b)–2(c) we show the time evolution of the abundances of both species in both patches in these first two regimes. Within this coexistence region, for $\Delta < A_{12}$, species 1 could in principle migrate to patch $\beta$. However, its motility is not activated because the competitive pressure exerted by species 2 never becomes sufficiently large. For $\Delta > A_{12}$, instead, the motility of species 1 cannot be activated regardless of the abundance of species 2, since the exponent of the sigmoid remains positive.

However, further increasing $\Delta$ prevents the weak species from escaping from patch $\alpha$, as Eq. (4) is no longer satisfied. Consequently, none of the species invades patch $\beta$ and the weak species becomes extinct in patch $\alpha$, as shown in Fig. 2(d). The boundary can be found analytically by setting $x_1 = K$ in Eq. (4), yielding $\Delta = A_{21}$ as $K = 1$.

We now separately relax the limits $\mu_0 \to 0$ and $\xi \to \infty$ to explore how increasing linear diffusion and reducing the steepness (and thus the nonlinearity in the competitor's abundance) of the motility response affect coexistence. When $\mu_0 \neq 0$, the fully segregated state (1,0,0,1) is no longer an exact steady state because baseline diffusion continuously transfers a small number of individuals to the opposite patch, leading to imperfectly segregated stationary states. However, these states are still stable and their stability originates from the same mechanism: Minority populations are maintained at low abundances by the balance between diffusion, competition, and the escape response, while resident populations relax toward their local carrying capacities. In the general case of finite $\xi$ and $\mu_0$, we have confirmed stability numerically by computing the eigenvalues of the full Jacobian matrix and verifying that all their real parts are negative.

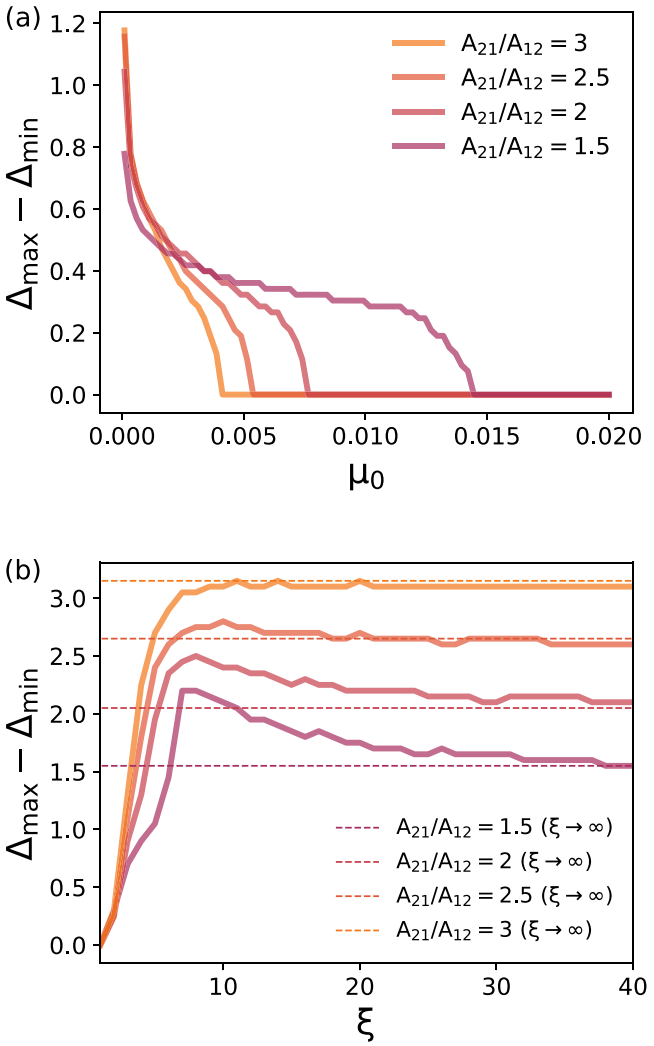



FIG. 3. (a) Range of motility thresholds, $\Delta_{\max} - \Delta_{\min}$, that permit segregated coexistence as a function of the linear diffusion rate $\mu_0$, shown for different values of the interspecific competition ratio $A_{21}/A_{12}$ and in the limit $\xi \to \infty$. (b) Range of motility thresholds, $\Delta_{\max} - \Delta_{\min}$, as a function of the steepness parameter $\xi$ of the sigmoidal escape response, again for fixed values of $A_{21}/A_{12}$ and in the limit $\mu_0 \to 0$. The dashed lines indicate the corresponding asymptotic values obtained in the limit $\xi \to \infty$. All curves in both panels are obtained from numerical integration of Eqs. (1) with parameters $A_{11} = A_{22} = 1$, $\mu_S = 0.1$, and $A_{12} = 1.1$.

In Fig. 3 we show how the coexistence interval in motility thresholds, $\Delta_{\max} - \Delta_{\min}$, changes as a function of $\mu_0$ [Fig. 3(a)] and $\xi$ [Fig. 3(b)], for different values of the ratio $A_{21}/A_{12}$. Increasing linear diffusion monotonically shrinks the coexistence range, which eventually vanishes ($\Delta_{\max} - \Delta_{\min} = 0$) once $\mu_0$ is sufficiently large. Figure 3(a) highlights the breakdown of the competition-colonization trade-off when linear diffusion becomes strong: For small diffusion, stronger asymmetry (larger $A_{21}/A_{12}$) enlarges the coexistence interval because it enhances the ability of species 2 to quickly escape and colonize patch $\beta$. In contrast, at higher

diffusion rates, asymmetry no longer favors coexistence, as it mainly amplifies the exploitation of species 2 by species 1. Consequently, less asymmetric interactions require larger values of $\mu_0$ to eradicate coexistence.

Regarding the influence of the steepness of the motility response, we show in Fig. 3(b) that coexistence range exhibits a sharp increase with $\xi$ before saturating at the asymptotic value reached in the limit $\xi \to \infty$ for all values of $A_{21}/A_{12}$. This behavior indicates that a minimum degree of nonlinearity in the escape response is required to sustain coexistence. In Appendix B, we provide theoretical arguments showing that segregated coexistence cannot occur when $\xi \to 0$ in the regime $A_{12} > 1$ and $A_{21} > 1$.

Interestingly, some curves in Fig. 3(b) exhibit a nonmonotonic behavior, with coexistence being maximized at an intermediate value of $\xi$. Further investigation of this behavior revealed an additional coexistence region at finite $\xi$, corresponding to $\Delta > A_{21}$. Recall that, in this region, the motility of species 2 is suppressed in the $\xi \to \infty$ limit. Decreasing $\xi$ reduces the sharpness of the motility function, allowing species 2 to move through an exponentially small diffusive flux to patch $\beta$, while the response remains sufficiently sharp to prevent the simultaneous movement of species 1. This promotes spatial segregation and, therefore, coexistence even for $\Delta > A_{21}$, increasing the range of $\Delta$ supporting coexistence compared with the $\xi \to \infty$ limit. Further decreasing $\xi$ eventually allows species 1 to move as well, thereby hampering spatial segregation and, consequently, coexistence.

Importantly, we do not consider this finite-$\xi$, $\Delta > A_{21}$ regime to be particularly informative for the mechanism investigated in this work, as coexistence here relies on small but persistent diffusive fluxes rather than on the interplay between species abundances, competitive interactions, and the activation of the adaptive escape response that characterizes the $\Delta < A_{21}$ regime.

In the next section, we extend this analysis to two-dimensional lattices of various sizes, showing that the simplified two-patch framework developed above remains to some extent informative in these more complex settings.

### C. Two-dimensional lattices

We now extend our analysis to more complex metapopulations beyond the two-patches system. To this end, we consider multiple two-dimensional lattices composed of $L \times L$ cells, and we vary the side length $L$. As $L$ increases, this can be interpreted either as an expansion of the available space or, equivalently, as a reduction of the characteristic spatial scale at which bacteria interact and grow locally. The equations describing this extended setting are identical to those in Eq. (1), with $M_{\alpha\beta} = M_{\beta\alpha} = 1/\mathcal{N}$ for neighboring cells, where $\mathcal{N}$ is the fixed number of neighbors of each cell, and $M_{\alpha\beta} = M_{\beta\alpha} = 0$ otherwise.

As before, we initialize the system by placing a small seed of both species in a single cell, specifically the central one, to mimic experiments in which a central inoculum spreads across a Petri dish or a plate. Likewise, we construct the mobility matrix $\mathbf{M}$ by assuming a Moore neighborhood, thus connecting each patch with each eight nearest neighbors in the lattice. In the Supplemental Material [27] we also analyze the case of more heterogeneous initial spatial distributions and other mobility matrix by setting a Von Neumann neighborhood, connecting each patch with each four nearest neighbors. In the following analysis we fix $\xi = 100$, as we have seen that the steepness of the sigmoid function favors coexistence. We also keep a nonzero diffusion term fixed at $\mu_0 = 10^{-3}$, the density-dependent motility rate at $\mu_S = 0.1$, and $A_{12} = 1.1$, while letting $A_{21}$ vary. These values were chosen not with a specific biological setup in mind but rather as those that better highlight the phenomenology that we are going to discuss in the following. In the Supplemental Material [27], we performed additional analyses varying all the parameters mentioned above, showing that, although some differences arise, the main phenomenology persists also in these other parameter regimes.

Figure 4 displays the same phase diagram shown in Fig. 2 expressed in terms of the ratio of competition coefficients $A_{21}/A_{12}$ and the activation threshold $\Delta$, for multiple values of the spatial dimension $L$. In contrast to Fig. 2, the heatmap here represents the total abundance difference $x_1 - x_2 = \sum_\alpha (x_1^\alpha - x_2^\alpha)$, between the two species at equilibrium, normalized by the total available area $L^2$, that we indicate with $\chi$. The darkest blue region corresponds to parameter combinations for which coexistence is not achieved, and only the stronger species 1 persists. The most evident feature is that increasing $L$ leads to a general expansion of the coexistence region. Intuitively, larger lattices provide more empty frontier for the faster-escaping species to colonize before diffusive inflow can reestablish local competitive exclusion, thereby strengthening the competition-colonization trade-off. Within this region, the dominance of one species over the other depends on several factors, although some clear patterns emerge. For small values of $\Delta$ and increasing ratios $A_{21}/A_{12}$, the system consistently transitions from complete dominance of species 1 (noncoexistence) to coexistence with comparable abundances of the two species (white or lightly shaded blue and red areas). When $L$ is small, the reddish regions in which species 2 dominates are a consequence of the reduced spatial structure of the system. For instance, in the case $L = 3$, the reddish region corresponds to the situation in which species 2 colonizes the unique concentric square surrounding the central patch, while species 1 remains confined to the latter. This configuration is essentially equivalent to the two-patch case, with the only difference that eight of the nine cells are colonized by species 2 instead of only one. As $L$ increases, coexistence becomes possible over a broader range of $\Delta$; in particular, for large $L$ and $\Delta \geqslant 1$, a region appears in which the weaker competitor, species 2, becomes largely dominant.

Remarkably, as the lattice size increases, the coexistence region approaches the phase diagram obtained in the two-patch system without standard diffusion ($\mu_0 = 0$), shown in Fig. 2 (the analytical prediction derived for that case is plotted as a dashed line in Fig. 4). This convergence suggests that a system with limited spatial extent (or, equivalently, with a large interaction range) but no diffusion, behaves similarly to a larger spatial system (or shorter-range interactions) and nonzero diffusion. In this sense, the theoretical description developed for the simpler two-patch setting also captures to some extent the behavior of this more realistic spatial framework.

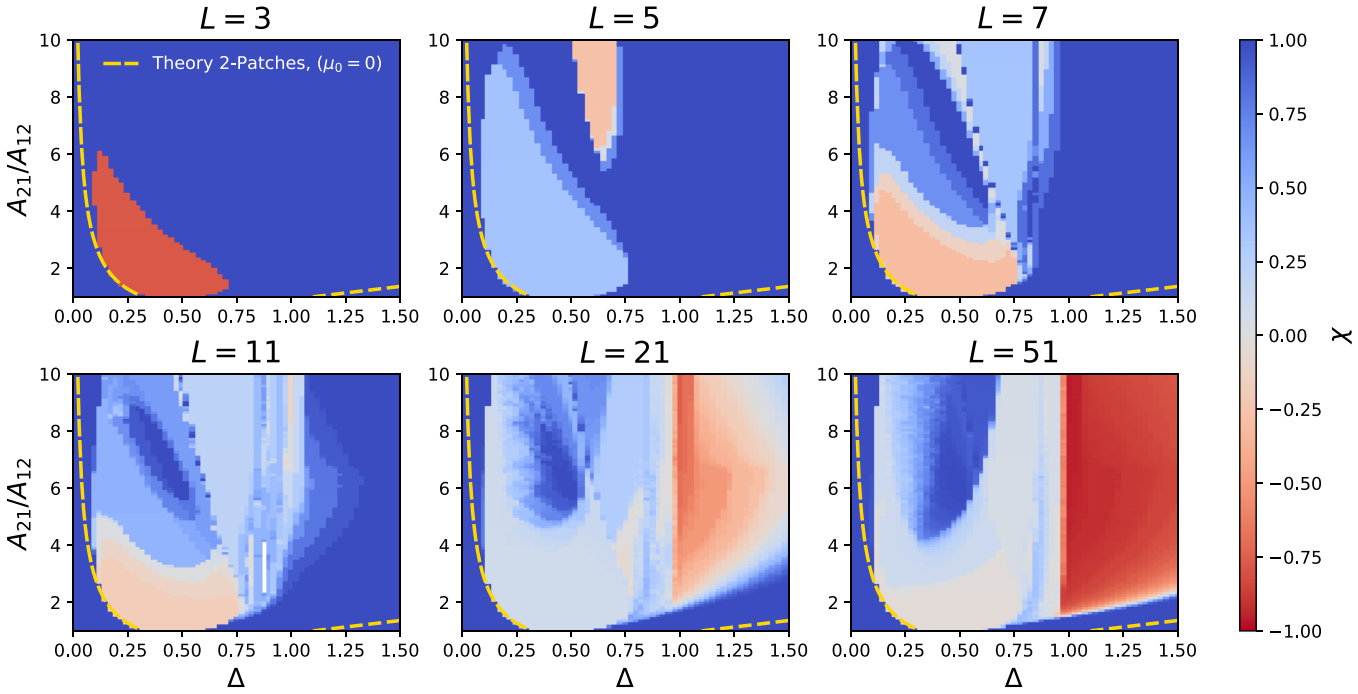



FIG. 4. Heatmaps for lattices with different side lengths ($L = 3, 5, 7, 11, 21, 51$) showing the equilibrium difference in total abundances between species 1, $x_1 = \sum_\alpha x_1^\alpha$, and species 2, $x_2 = \sum_\alpha x_2^\alpha$. This difference is normalized by the total available area $L \times L$ and we call the normalized difference $\chi \equiv (x_1 - x_2)/L^2$. Blueish regions indicate dominance of species 1, whereas reddish regions indicate dominance of species 2. As in Fig. 2, the activation threshold $\Delta$ is reported on the $x$ axis and the ratio of competition coefficients $A_{21}/A_{12}$ on the $y$ axis. The gold dashed line represents the analytical prediction obtained for the two-patch case without linear diffusion (see Fig. 2). Each cell in the heatmap corresponds to a numerical integration of Eq. (1) with parameter values $A_{11} = A_{22} = 1$, $A_{12} = 1.1$, $\xi = 100$, $\mu_0 = 0.001$, and $\mu_S = 0.1$. Initial conditions are $x_1^\alpha(0) = x_2^\alpha(0) = 0.001$ in the central cell and zero elsewhere. For all lattices, the mobility matrices $\mathbf{M}$ are constructed considering a Moore neighborhood. In the Supplemental Material [27] we show the same heatmaps changing initial conditions, type of neighborhood and the chosen fixed values for $A_{12}$, $\xi$, $\mu_0$, and $\mu_S$.

To further examine these results, Figs. 5(a)–5(c) show how the equilibrium abundances of the two species vary with increasing interspecific competition for three different values of the motility threshold: $\Delta = 0.6$ [Fig. 5(a)], $\Delta = 0.8$ [Fig. 5(b)], and $\Delta = 1.0$ [Fig. 5(c)]. These results illustrate how the interplay between Lotka-Volterra demographic dynamics and nonlinear motility responses leads to qualitatively different effects of increasing interspecific competition on coexistence. Depending on the value of $\Delta$, increasing the ratio $A_{21}/A_{12}$ can (i) reduce the abundance of the weaker species [Fig. 5(a)], (ii) promote coexistence with comparable spatial abundances of the two species [Fig. 5(b)], or (iii) even lead to the spatial dominance of the weaker competitor over the stronger one [Fig. 5(c)].

To understand the disparate effect of interspecific competition, we explicitly study the spatial self-organization of the species by plotting representative spatial patterns observed at equilibrium for $\Delta = 0.6$ [Fig. 5(d)], $\Delta = 0.8$ [Fig. 5(e)], $\Delta = 1$ [Fig. 5(f)] and different values of $A_{21}/A_{12}$. In the coexistence regime with $\Delta < 1$, we consistently observe the emergence of concentric rings in which the two species alternate in space. This organization arises because, for small $\Delta$, the density-dependent motilities of both species eventually gets activated. Since $A_{12} < A_{21}$, species 2 reaches its activation threshold first and escapes outward, colonizing the first ring around the central cell, while species 1 diffuses more slowly with $\mu_0$. In this newly occupied ring, species 2 attains a density high enough to trigger the escape response of species 1, which then fills the next outer ring. This process repeats, producing alternating concentric domains of the two species.

As the competitive effect of species 1 on species 2 increases (i.e., for larger values of $A_{21}/A_{12}$), the concentric rings become destabilized and give rise to more irregular spatial patterns. This occurs because, under sufficiently strong competition, the small inflow of species 1 generated by the diffusion term $\mu_0$ can locally out-compete species 2 even where species 2 is initially more abundant [Fig. 5(d)].

When $\Delta$ approaches 1, a different mechanism becomes relevant. For low values of $A_{21}/A_{12}$, the density-dependent motility of species 2 activates too late, and it may fail to survive. In this regime, stronger competition is required for species 2 to reach the activation threshold early enough to escape and re-establish the concentric rings pattern, as shown in Fig. 5(e).

Finally, when $\Delta \geqslant 1$, the escape response of species 1 is hardly activated, and its spread is limited to standard diffusion. In contrast, species 2 escapes more rapidly as $A_{21}/A_{12}$ increases, colonizing regions farther from the center. Stronger competition leaves species 1 progressively less time to expand before species 2 establishes itself. This regime is shown in Fig. 5(f) and it is particularly notable because species 2, despite being the inferior competitor, becomes substantially more abundant and occupies a larger spatial region than species 1. This counterintuitive behavior can be traced back

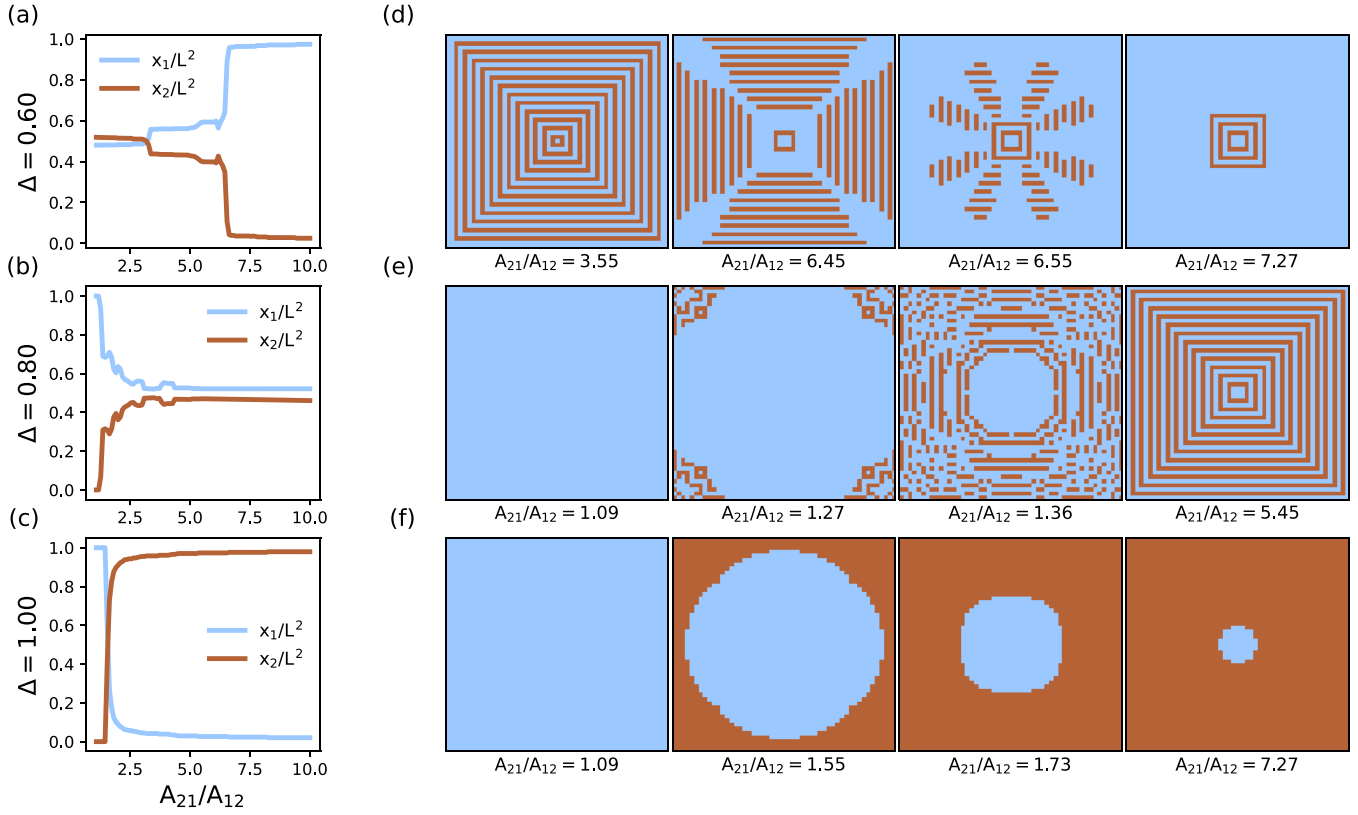



FIG. 5. [(a)–(c)] Final total abundances of species 1 ($x_1$) and species 2 ($x_2$), normalized by the lattice size $L^2$, as a function of $A_{21}/A_{12}$, for three values of the activation thresholds $\Delta = 0.60,\ 0.80,\ 1.00$. [(d)–(f)] Stationary spatial patterns for species 1 (blue) and species 2 (red) on a two-dimensional lattice with side length $L = 51$. Rows correspond to activation thresholds $\Delta = 0.60,\ 0.80,\ 1.00$, and columns to increasing values of the competition ratio $A_{21}/A_{12}$. All results are obtained from numerical integration of the model with parameters $A_{11} = A_{22} = 1$, $A_{12} = 1.1$, $\xi = 100$, $\mu_0 = 0.001$, and $\mu_S = 0.1$. Initial conditions place both species at density 0.001 in the central cell and zero elsewhere. The mobility matrix **M** is constructed considering a Moore neighborhood.

to the colonization–exploitation trade-off, whereby enhanced motility allows the weaker species to preferentially occupy empty spatial patches.

## III. DISCUSSION

Microbial communities display both high taxonomic diversity and remarkable long-term stability in composition [28,29]. This empirical evidence has motivated sustained theoretical efforts to extend classical ecological models, such as Lotka-Volterra and consumer-resource frameworks, which generally predict that increasing diversity leads to instability [30]. One line of explanation reconciles diversity and stability by assuming weak or sparse interactions between species [31,32]. An alternative view is that classical ecological frameworks are overly reductionist and lack key ingredients required to account for the observed levels of diversity. From this perspective, incorporating explicit spatial structure emerges as a promising direction [33], as microbial communities are typically far from well mixed at local scales and instead exhibit pronounced patchiness and spatial segregation among species [34–36].

In this work, we show that, in a spatially structured model, coexistence among strongly competing species can be sustained by an escape response in which motility increases nonlinearly with the local abundance of competitors. In the competitive-exclusion regime ($A_{12} > 1$ and $A_{21} > 1$), coexistence does not occur within single patches, and therefore persistence at the metapopulation level relies on spatial self-organization. In our framework, coexistence arises via a classical competition-colonization trade-off, which emerges from coupling demographic interactions to the sigmoidal, quorum-sensing-like functional form assumed for the escape response. In this setting, a high ability to escape from competitors also entails an increased susceptibility to being outcompeted, and coexistence relies on a balance between these opposing effects. If the inferior competitor grows too rapidly, then it can trigger the escape of the superior competitor, ultimately leading to exclusion; conversely, if it grows too slowly, then it risks being outcompeted, again resulting in exclusion. This interplay is what generates the rich phenomenology in the phase diagrams discussed previously.

The role of spatial segregation in promoting coexistence has a long history in theoretical ecology. In one of the first works in this direction, Levin [37] showed that, in patchy environments, linear diffusive fluxes can have a stabilizing effect on the coexistence of competing species. In that framework, however, coexistence relied primarily on initial heterogeneity in patch colonization combined with sufficiently low diffusion rates. Subsequent work introduced nonlinearities in migration by allowing dispersal to depend explicitly on competitor densities, as in Shigesada *et al.* [38] and Mimura and Kawasaki

[39]. In these models, the effect was typically implemented through terms proportional to the product of species abundances (e.g., $-c\,x_1^\alpha x_2^\alpha$, with $c$ a coupling constant). As in our case, these studies showed that nonlinear migration can enable coexistence in regimes where it is otherwise forbidden in well-mixed systems.

In all these aforementioned approaches, growth, competition, and migration are typically decoupled, allowing coexistence to be recovered by independently tuning motility parameters. A key difference in our approach is that competition and motility are not tuned independently: The same interspecific interaction coefficients that determine demographic suppression also enter the escape response. Moreover, motility dependence on competitor abundance is strongly nonlinear, being mediated by the sigmoid function. In the limit $\xi \to 0$, this formulation reduces to the linear (in terms of competitor's abundance) models discussed above and coexistence is no longer observed within our coupled setup [Fig. 3(b) and Appendix B]. In our case, the weaker competitor is not endowed *a priori* with a higher colonization ability (especially when $A_{12} \sim A_{21}$). Instead, the competition-colonization trade-off emerges spontaneously from the growth dynamics: The stronger competitor grows faster and therefore activates the escape response of the weaker one earlier. This asymmetry arises solely from the nonlinear, threshold-like nature of the escape response, which is essential for the emergence of coexistence in our framework.

In ecology, near-perfect reciprocal exclusion of species across sites, leading to alternating patches, is commonly referred to as a checkerboard distribution [40]. The origins of checkerboard distributions have long been debated [41]. While they are often interpreted as signatures of interspecific competition [42], it has also been argued that similar patterns may arise purely from environmental filtering, even in the absence of direct interactions [43]. Our results identify an additional mechanism through which competition, when coupled to a strongly nonlinear escape response, can both generate and maintain checkerboard-like spatial organization.

Beyond coexistence, we have also shown the emergence of rich spatial pattern formation in lattice geometries as a function of the motility threshold and the interspecific competition. Several of the coexistence and spatial segregation patterns predicted by our model have also been observed experimentally. In particular, the concentric ring structures arising from the reciprocal activation of motility in two competing species have been previously observed both *in silico* and experimentally by Curatolo *et al.* [11]. Moreover, Gude *et al.* [44] experimentally observed that a competition-colonization trade-off can promote coexistence through reciprocal spatial exclusion, whereby the faster grower colonizes the center of the colony while the faster migrator colonizes the surrounding empty space, qualitatively resembling the coexistence patterns observed in our model for $\Delta > 1$. Interestingly, they also showed that the locally disadvantaged species may become globally dominant in abundance, as observed in our model. While in their case the competition-colonization trade-off originates from intrinsic phenotypic differences between the two species, in our model it emerges dynamically from coupling competition with an escape response. Despite these mechanistic differences, both works highlight the fundamental role of competition, colonization dynamics, and space in promoting coexistence between strong competitors. We believe that these experimental observations provide further support for the general ecological mechanism highlighted by our theoretical framework.

While we have adopted a discrete-space metapopulation framework, continuous-space descriptions are equally legitimate alternatives. At the most detailed level, microbial populations with motility-mediated interactions can be described by nonlocal integropartial differential equations, where individuals continuously interact over finite spatial scales. Such formulations are, however, mathematically intricate and typically require additional approximations to become analytically tractable. In particular, classical active-matter frameworks describing MIPS-like behavior usually rely on coarse-grained continuum equations obtained by assuming smooth density fields and approximating nonlocal interactions through local or gradient-expansion terms.

In contrast, metapopulation models perform the coarse-graining directly in space by partitioning the system into discrete patches connected by migration. This approach naturally accounts for interactions occurring over finite spatial scales through patch-level processes while retaining a relatively intuitive and analytically tractable description based on coupled ordinary differential equations. Such tractability is one of the reasons why metapopulation models are the standard framework in theoretical ecology when the primary focus is on coexistence, persistence and diversity rather than on microscopic pattern formation [45–47]. The price paid for this simplification is the assumption that populations are locally well mixed within each patch and that demographic interactions occur at the mesoscopic scale set by the patch size. The plausibility of this assumption naturally depends on both the biological system and the spatial scale of interest. Microbial environments are often intrinsically patchy or porous or, even in homogeneous environments, microorganisms can spontaneously self-organize into spatially segregated microcolonies. Moreover, questions concerning coexistence and diversity typically concern intermediate-to-large spatial scales rather than microscopic ones. At these scales, reducing the spatial resolution through a discrete description may not necessarily imply a significant loss of ecological information.

In conclusion, the theoretical framework here introduced represents one of the first attempts to frame the exploitation-colonization trade-off as the natural coupling between demographic interactions and motility responses driven by quorum-sensing like mechanisms. In a broader perspective, our findings are relevant to two closely related yet distinct research directions: the identification of mechanisms that promote coexistence in microbial ecology, and the introduction of a spatial framework that generates novel patterns of relevance to active-particle physics.

## ACKNOWLEDGMENTS

We acknowledge support from Spanish Ministry of Science, Innovation and Universities (MICIU), the Spanish State Research Agency (AEI), and the European Regional Development Fund (ERDF/EU),

under Grant (PID2024-158120NB-C21), Generalitat de Catalunya (2021SGR-00633) and ICREA Academia. This project has received funding from the European Union's Horizon 2020 research and innovation programme under the Marie Skłodowska-Curie Grant Agreement No. 945413 and from the Universitat Rovira i Virgili (URV).

M.M., D.S.-P., and A.A. designed the study; M.M. performed analysis, mathematical calculations, and wrote code; all the authors wrote the paper and discussed the results.

## DATA AVAILABILITY

There are no publicly available research data or software supporting this manuscript. Requests for further information or data should be sent to the authors.

## APPENDIX A: ANALYTICAL DESCRIPTION FOR THE TWO-PATCH SETTING ($\xi \to \infty$, $\mu_0 \to 0$)

We recall the two-patch scenario in which two species, labeled 1 and 2, inhabit two connected but distinct patches, $\alpha$ and $\beta$, whose dynamics follow Eq. (1). Throughout this appendix we consider the limits $\xi \to \infty$ and $\mu_0 \to 0$, so that the motility function reduces to a step function. As already mentioned in the main text, we start from an initial condition where a small seed of both species is present only in patch $\alpha$, while patch $\beta$ is initially empty.

In this regime, stable coexistence can occur only if the inferior competitor, here species 2, activates the escape response and colonizes patch $\beta$, while species 1 does not. We recall that this requirement is equivalent to imposing the conditions established Eqs. (3) and (4). The second condition is automatically satisfied if $A_{21} < \Delta$, since species 1 always dominates locally and reaches the carrying capacity $K = 1$. To determine when the first condition holds, we must compute explicitly the time evolution of $x_2^\alpha(t)$ for all $t$. In order to do so, we approximate the equation for species 1 in patch $\alpha$ as

$$\frac{dx_1^\alpha(t)}{dt} = x_1^\alpha(t)\left(1 - x_1^\alpha(t) - A_{12}\,\epsilon\right), \tag{A1}$$

where we have replaced $x_2^\alpha(t)$ with a small constant value $\epsilon$. This approximation is valid when species 2 activates the escape response sufficiently early, so that species 1 experiences only weak competitive pressure arising from the low abundance of species 2. With this simplification and rewriting

$$\frac{1}{x_1^\alpha(t)\left(1 - x_1^\alpha(t) - A_{12}\,\epsilon\right)} = \frac{1}{1-\epsilon}\left(\frac{1}{x_1^\alpha(t)} + \frac{1}{1 - x_1^\alpha(t) - A_{12}\,\epsilon}\right),$$

we can easily integrate Eq. (A1), yielding

$$x_1^\alpha(t) = \frac{(1 - A_{12}\,\epsilon)}{1 + \left(\frac{1 - x_1^\alpha(0) - A_{12}\,\epsilon}{x_1^\alpha(0)}\right) e^{-t(1 - A_{12}\,\epsilon)}}, \tag{A2}$$

which is a shifted logistic form. With this we can now express explicity the time $\tau$ at which $x_1^\alpha(\tau) = \Delta/A_{21}$, i.e., the time at which the escape response is activated and species 2 starts to migrate towards patch $\beta$. After some algebra

$$x_1^\alpha(\tau) = \frac{\Delta}{A_{21}} \iff \tau = \frac{1}{1 - A_{12}\,\epsilon} \times \ln\left[\frac{\Delta}{A_{21}} \frac{\left(1 - x_1^\alpha(0) - A_{12}\,\epsilon\right)/x_1^\alpha(0)}{1 - A_{12}\,\epsilon - \Delta/A_{21}}\right]. \tag{A3}$$

For $t < \tau$, the variable $x_2^\alpha(t)$ experiences neither in-migration nor out-migration and therefore evolves solely according to the Lotka-Volterra dynamics

$$\frac{dx_2^\alpha(t < \tau)}{dt} = x_2^\alpha(t)\left(1 - x_2^\alpha(t) - A_{21}\,x_1^\alpha(t)\right). \tag{A4}$$

Since the coupling between $x_1^\alpha(t)$ and $x_2^\alpha(t)$ has been removed in Eq. (A1), this equation becomes a quadratic Bernoulli differential equation, which can be solved explicitly. By defining

$$E(t) \equiv \exp\left[\int_0^t \left(1 - A_{21} x_1^\alpha(t')\right) dt'\right], \tag{A5}$$

and applying a simple change of variables, one finds that the solution can be written as

$$x_2^\alpha(t < \tau) = \frac{E(t)}{1/x_2^\alpha(0) + \int_0^t E(t')\,dt'}. \tag{A6}$$

In our setup, both $E(t)$ and its integral can be computed explicitly. The first one, after a simple change of variables, reduces to an elementary integral and yields

$$E(t) = e^t \left(\frac{x_0\left(e^{t(1 - A_{12}\,\epsilon)} - 1\right) - A_{12}\,\epsilon + 1}{1 - A_{12}\,\epsilon}\right)^{-A_{21}}, \tag{A7}$$

where, for simplicity, we have introduced the shorthand notation $x_1^\alpha(0) = x_2^\alpha(0) \equiv x_0$. The time integral of the latter can be written as

$$\int_0^t E(t')\,dt' = (1 - A_{12}\,\epsilon)^{A_{21}} \int_0^t \frac{e^{t'}}{\left[x_0\left(e^{t'(1 - A_{12}\,\epsilon)} - 1\right) - A_{12}\,\epsilon + 1\right]^{A_{21}}} dt', \tag{A8}$$

which has a known solution in terms of incomplete beta functions $B_x(a, b)$ [48]:

$$\int_0^t E(t')\,dt' = (1 - A_{12}\,\epsilon - x_0)^{\frac{1 - A_{21} + A_{12}A_{21}\epsilon}{1 - A_{12}\epsilon}} (1 - A_{12}\,\epsilon)^{A_{21} - 1}\, x_0^{-\frac{1}{1 - A_{12}\epsilon}} \left[B_{X_{t'}}\left(\frac{1}{1 - A_{12}\,\epsilon}, \frac{A_{21} - \epsilon\, A_{12}A_{21} - 1}{1 - A_{12}\,\epsilon}\right)\right]_{t'=0}^{t'=t}, \tag{A9}$$

where

$$X_{t'} \equiv \frac{x_0\, e^{(1 - A_{12}\epsilon)t'}}{1 - A_{12}\epsilon - x_0\left(1 - e^{(1 - A_{12}\epsilon)t'}\right)}. \tag{A10}$$

Substituting expressions (A7) and (A9) into Eq. (A6), we obtain a complete description of $x_2^\alpha(t)$ for $t < \tau$. At $t = \tau$, the dynamics of $x_2^\alpha(t)$ changes due to the appearance of a migration term, $-\mu_S\, x_2^\alpha(t)$, representing the flux from patch $\alpha$ toward patch $\beta$.

Therefore, for $t > \tau$, the evolution is given by

$$x_2^\alpha(t > \tau) = x_2^\alpha(t)\big(1 - x_2^\alpha(t) - A_{21}x_1^\alpha(t) - 2\mu_S\, x_2^\alpha(t)\big), \tag{A11}$$

which is again a Bernoulli equation, and its solution has the same structure as in (A6). The procedure is identical to the previous case, but with a modified integrating factor $E'(t)$ and its corresponding integral, both affected by the migration term and by the fact that integration now starts at $t = \tau$. Explicitly,

$$E'(t) = e^{(t-\tau)(1-2\mu_S)}\left(\frac{e^{t(1-A_{12}\epsilon)} + (1 - x_0 - \epsilon)/x_0}{e^{\tau(1-A_{12}\epsilon)} + (1 - x_0 - \epsilon)/x_0}\right)^{-A_{21}} \tag{A12}$$

and

$$\int_\tau^t E'(t')\,dt' = \frac{e^{\tau(2\mu_S-1)}}{(e^{\tau(1-A_{12}\epsilon)} + (1 - x_0 - A_{12}\epsilon)/x_0)^{-A_{21}}}\frac{1}{1 - A_{12}\epsilon}\left(\frac{1 - A_{12}\epsilon - x_0}{x_0}\right)^{\frac{1-2\mu_S-A_{21}+\epsilon A_{12}A_{21}}{1-A_{12}\epsilon}} \times \left[B_{X'_{t'}}\left(\frac{1 - 2\mu_S}{1 - A_{12}\epsilon}, \frac{A_{21} - \epsilon A_{12}A_{21} + 2\mu_S - 1}{1 - A_{12}\epsilon}\right)\right]_{t'=\tau}^{t'=t}, \tag{A13}$$

with

$$X'_{t'} \equiv \frac{e^{(1-A_{12}\epsilon)t'}}{e^{(1-A_{12}\epsilon)t'} + \frac{1-A_{12}\epsilon-x_0}{x_0}}. \tag{A14}$$

With $E'(t)$ and $\int_\tau^t E(t')\,dt'$, we can compute $x_2^\alpha(t)$ for $t \geqslant \tau$ again as

$$x_2^\alpha(t \geqslant \tau) = \frac{E'(t)}{1/x_2^\alpha(\tau) + \int_\tau^t E(t')\,dt'}, \tag{A15}$$

where $x_2^\alpha(\tau)$ is obtained from the previous phase [Eq. (A6)], together with the explicit formula for $\tau$ [Eq. (A3)].

With these expressions at hand, it is possible to determine which combinations of parameters lead to coexistence through segregation. Indeed, the theoretical curves shown in Figs. 2 and 4 are obtained by computing the minimum value of $\Delta$ for which condition (3), namely

$$x_2^\alpha(t) < \Delta/A_{12}, \quad \forall t,$$

is satisfied, using $x_2^\alpha(t)$ from Eq. (A15). All the curves depicted in the figures in the main text are obtained considering $\epsilon = 0.05$.

## APPENDIX B: THE LIMIT $\xi \to 0$

Here we analyze the limit in which the sigmoidal escape response becomes linear in the competitor abundance, corresponding to $\xi \to 0$. For small argument $x$, the sigmoid admits the expansion

$$\frac{1}{1 + e^x} = \frac{1}{2} - \frac{x}{4} + \mathcal{O}(x^3). \tag{B1}$$

Applying this expansion, for instance, to the motility rate of species 1 from patch $\alpha$ to $\beta$, we obtain to leading order

$$\mu_1^{\alpha\beta}(t) \simeq M_{\alpha\beta}\left[\mu_0 + 2\mu_S\left(\frac{1}{2} - \frac{\xi\Delta}{4} + \frac{\xi A_{12}\, x_2^\alpha(t)}{4}\right)\right]. \tag{B2}$$

With this approximation, the system of four equations describing the two-patch model becomes analytically tractable. We investigate whether segregated coexistence remains possible in this linearized limit, i.e., whether a steady state of the form

$$\big(x_1^\alpha, x_1^\beta, x_2^\alpha, x_2^\beta\big) = (1 - \epsilon_1,\ \epsilon_1,\ \epsilon_2,\ 1 - \epsilon_2), \quad \epsilon_1, \epsilon_2 \ll 1,$$

can exist.

Linearizing the steady-state equations and solving those for $x_1^\alpha$ and $x_1^\beta$, we obtain

$$\epsilon_1 = \frac{\mu_S(2 - \xi\Delta)}{2[\mu_S(2 - \xi\Delta) + (\xi\mu_S + 1)(A_{12} - 1)]}, \tag{B3}$$

and

$$\epsilon_2 = \frac{\mu_S(2 - \xi\Delta)(2 - A_{12})}{2A_{12}[\mu_S(2 - \xi\Delta) + (\xi\mu_S + 1)(A_{12} - 1)]} = \left(\frac{2}{A_{12}} - 1\right)\epsilon_1, \tag{B4}$$

where, for readability, we have taken the limit $\mu_0 \to 0$.

Two trivial cases leading to full segregation are already apparent. The first corresponds to $\mu_S = 0$, for which no motility is present and segregation can only persist if it is imposed by the initial conditions. The second occurs when $\xi\Delta = 2$, which in the limit $\xi \to 0$ requires $\Delta \to \infty$.

We next focus on the nontrivial case $\epsilon_1 > 0$ and $\epsilon_2 > 0$. From Eqs. (B3) and (B4), this requires

$$\begin{cases} 2 - \xi\Delta > 0, \\ A_{12} < 2, \end{cases} \quad \text{or} \quad \begin{cases} 2 - \xi\Delta < \frac{(\xi\mu_S+1)(A_{12}-1)}{\mu_S}, \\ A_{12} < 2. \end{cases} \tag{B5}$$

Substituting Eqs. (B3) and (B4) into the linearized equations for species 2, denoted by $E_3$ and $E_4$, we obtain:

$$E_3 = -\epsilon_1 P, \quad E_4 = -\epsilon_1\big[P + 2(A_{12} + A_{21} - 2)\big], \tag{B6}$$

with

$$P = (A_{12} + A_{21} - 2)[A_{12} + \xi\mu_0(1 - \Delta)(A_{12} - 1)] + (A_{12} - 1)[A_{12} + \xi\mu_0(1 - \Delta)]. \tag{B7}$$

A steady configuration, i.e. $E_3 = 0$ and $E_4 = 0$ can only appear if $A_{12} + A_{21} = 2$, which lies outside our competitive exclusion regime ($A_{12} > 1$, $A_{21} > 1$). We therefore conclude that, within our coupled framework, the limit $\xi \to 0$ does not permit segregated coexistence. This result confirms the numerical findings shown in Fig. 3(b) and demonstrates that a strongly nonlinear, thresholdlike escape response is a necessary ingredient for coexistence.

## APPENDIX C: NUMERICAL INTEGRATION DETAILS

All numerical results presented in the manuscript are obtained by integrating the dynamical equations using the adaptive Runge-Kutta method RK45, as implemented in `solve_ivp` from `SciPy`. Relative and absolute tolerances are set to $10^{-6}$ and $10^{-8}$, respectively, and the maximum allowed integration step is fixed to 0.1. We have also established at each integration step a lower bound for species abundances equal to $10^{-6}$. Simulations are evolved up to when a stationary state is reached. More specifically, stationarity is defined by the condition

$$\max_i \left| \frac{dy_i}{dt} \right| < 10^{-9},$$

where the maximum is taken over all dynamical variables of the system.


[1] N. Wadhwa and H. Berg, Bacterial motility: Machinery and mechanisms, Nat. Rev. Microbiol. **20**, 161 (2022).

[2] E. Budrene and H. Berg, Complex patterns formed by motile cells of *Escherichia coli*, Nature (London) **349**, 630 (1991).

[3] C. M. Waters and B. L. Bassler, Quorum sensing: Cell-to-cell communication in bacteria, Annu. Rev. Cell Dev. Biol. **21**, 319 (2005).

[4] R. Daniels, J. Vanderleyden, and J. Michiels, Quorum sensing and swarming migration in bacteria, FEMS Microbiol. Rev. **28**, 261 (2004).

[5] H. H. Hoang, N. Gurich, and J. E. González, Regulation of motility by the expr/sin quorum-sensing system in *Sinorhizobium meliloti*, J. Bacteriol. **190**, 861 (2008).

[6] R. F. Kinsinger, M. C. Shirk, and R. Fall, Rapid surface motility in Bacillus subtilis is dependent on extracellular surfactin and potassium ion, J. Bacteriol. **185**, 5627 (2003).

[7] G. Cárcamo-Oyarce, P. Lumjiaktase, R. Kümmerli, and L. Eberl, Quorum sensing triggers the stochastic escape of individual cells from Pseudomonas putida biofilms, Nat. Commun. **6**, 5945 (2015).

[8] R. Daniels, S. Reynaert, H. Hoekstra, C. Verreth, J. Janssens, K. Braeken, M. Fauvart, S. Beullens, C. Heusdens, I. Lambrichts, D. E. De Vos, J. Vanderleyden, J. Vermant, and J. Michiels, Quorum signal molecules as biosurfactants affecting swarming in Rhizobium etli, Proc. Natl. Acad. Sci. USA **103**, 14965 (2006).

[9] J. Tailleur and M. E. Cates, Statistical mechanics of interacting run-and-tumble bacteria, Phys. Rev. Lett. **100**, 218103 (2008).

[10] M. E. Cates and J. Tailleur, Motility-induced phase separation, Annu. Rev. Condens. Matter Phys. **6**, 219 (2015).

[11] A. I. Curatolo, N. Zhou, Y. Zhao, C. Liu, A. Daerr, J. Tailleur, and J. Huang, Cooperative pattern formation in multi-component bacterial systems through reciprocal motility regulation, Nat. Phys. **16**, 1152 (2020).

[12] A. Dinelli, J. O'Byrne, A. Curatolo, Y. Zhao, P. Sollich, and J. Tailleur, Non-reciprocity across scales in active mixtures, Nat. Commun. **14**, 7035 (2023).

[13] Y. Duan, J. Agudo-Canalejo, R. Golestanian, and B. Mahault, Dynamical pattern formation without self-attraction in quorum-sensing active matter: The interplay between nonreciprocity and motility, Phys. Rev. Lett. **131**, 148301 (2023).

[14] W. J. M. Ridgway, M. P. Dalwadi, P. Pearce, and S. J. Chapman, Motility-induced phase separation mediated by bacterial quorum sensing, Phys. Rev. Lett. **131**, 228302 (2023).

[15] A. Dinelli, A. Altieri, and J. Tailleur, Random motility regulation drives the fragmentation of microbial ecosystems, Phys. Rev. E **114** 014404 (2026).

[16] M. Mattei, D. Soriano-Paños, M. Halappanavar, and A. Arenas, Structured interactions drive abrupt transitions in the spatial organization of microbial communities, Phys. Rev. Res. **7**, 043210 (2025).

[17] O. Hallatschek, S. S. Datta, K. Drescher, J. Dunkel, J. Elgeti, B. Waclaw, and N. S. Wingreen, Proliferating active matter, Nat. Rev. Phys. **5**, 407 (2023).

[18] K. Z. Coyte, J. Schluter, and K. R. Foster, The ecology of the microbiome: Networks, competition, and stability, Science **350**, 663 (2015).

[19] P. Chesson, Mechanisms of maintenance of species diversity, Annu. Rev. Ecol. Syst. **31**, 343 (2000).

[20] P. Amarasekare, Competitive coexistence in spatially structured environments: A synthesis, Ecol. Lett. **6**, 1109 (2003).

[21] B. M. Bolker and S. W. Pacala, Spatial moment equations for plant competition: Understanding spatial strategies and the advantages of short dispersal, Am. Nat. **153**, 575 (1999).

[22] T. K. Fuller and L. B. Keith, Non-overlapping ranges of coyotes and wolves in northeastern Alberta, J. Mammal. **62**, 403 (1981).

[23] H. Webster, J. W. McNutt, and K. McComb, African wild dogs as a fugitive species: Playback experiments investigate how wild dogs respond to their major competitors, Ethology **118**, 147 (2012).

[24] S. M. Durant, Living with the enemy: Avoidance of hyenas and lions by cheetahs in the Serengeti, Behav. Ecol. **11**, 624 (2000).

[25] M. E. Cates, D. Marenduzzo, I. Pagonabarraga, and J. Tailleur, Arrested phase separation in reproducing bacteria creates a generic route to pattern formation, Proc. Natl. Acad. Sci. USA **107**, 11715 (2010).

[26] M. Mattei and A. Arenas, Exploring spatial segregation induced by competition avoidance as driving mechanism for emergent coexistence in microbial communities, Phys. Rev. E **110**, 014404 (2024).

[27] See Supplemental Material at http://link.aps.org/supplemental/10.1103/4t9n-nvgc for additional analyses including heterogeneous initial conditions, alternative neighborhood structures, a different motility function, and variations of the model parameters $(A_{12})$, $(\xi)$, $(\mu_0)$, and $(\mu_S)$.

[28] L. R. Thompson, J. G. Sanders, D. McDonald, A. Amir, J. Ladau, K. J. Locey, R. J. Prill, A. Tripathi, S. M. Gibbons, G. Ackermann, J. A. Navas-Molina, S. Janssen, E. Kopylova, Y. Vázquez-Baeza, A. González, J. T. Morton, S. Mirarab, Z. Zech Xu, L. Jiang, M. F. Haroon, *et al.*, A communal catalogue reveals earth's multiscale microbial diversity, Nature (London) **551**, 457 (2017).

[29] T. H. M. P. Consortium, Structure, function and diversity of the healthy human microbiome, Nature (London) **486**, 207 (2012).

[30] R. M. May, Will a large complex system be stable? Nature (London) **238**, 413 (1972).
[31] J. Grilli, Macroecological laws describe variation and diversity in microbial communities, Nat. Commun. **11**, 4743 (2020).
[32] J. Camacho-Mateu, A. Lampo, M. Sireci, M. A. Muñoz, and J. A. Cuesta, Sparse species interactions reproduce abundance correlation patterns in microbial communities, Proc. Natl. Acad. Sci. USA **121**, e2309575121 (2024).
[33] O. X. Cordero and M. S. Datta, Microbial interactions and community assembly at microscales, Curr. Opin. Microbiol. **31**, 227 (2016).
[34] S. L. O'Brien, S. M. Gibbons, S. M. Owens, J. Hampton-Marcell, E. R. Johnston, J. D. Jastrow, J. A. Gilbert, F. Meyer, and D. A. Antonopoulos, Spatial scale drives patterns in soil bacterial diversity, Environ. Microbiol. **18**, 2039 (2016).
[35] R. U. Sheth, M. Li, W. Jiang, P. A. Sims, K. W. Leong, and H. H. Wang, Spatial metagenomic characterization of microbial biogeography in the gut, Nat Biotechnol **37**, 877 (2019).
[36] K. J. Welch, A. Liebman-Peláez, and E. I. Corwin, Biogeography of a human oral microbiome at the micron scale, Proc. Natl. Acad. Sci. USA **113**, 10807 (2016).
[37] S. A. Levin, Dispersion and population interactions, Am. Nat. **108**, 207 (1974).
[38] N. Shigesada, K. Kawasaki, and E. Teramoto, Spatial segregation of interacting species, J. Theor. Biol. **79**, 83 (1979).
[39] M. Mimura and K. Kawasaki, Spatial segregation in competitive interaction-diffusion equations, J. Math. Biol. **9**, 49 (1980).
[40] L. Stone and A. Roberts, The checkerboard score and species distributions, Oecologia **85**, 74 (1990).
[41] T. Dallas, B. A. Melbourne, and A. Hastings, When can competition and dispersal lead to checkerboard distributions? J. Anim. Ecol. **88**, 269 (2019).
[42] J. M. Diamond, Assembly of species communities, in *Ecology and Evolution of Communities*, edited by M. L. Cody and J. M. Diamond (Harvard University Press, Cambridge, MA, 1975), pp. 342–444.
[43] E. F. Connor and D. Simberloff, The assembly of species communities: Chance or competition? Ecology **60**, 1132 (1979).
[44] S. Gude, E. Pinçe, K. M. Taute, A.-B. Seinen, T. S. Shimizu, and S. J. Tans, Bacterial coexistence driven by motility and spatial competition, Nature (London) **578**, 588 (2020).
[45] D. Gravel, F. Massol, and M. Leibold, Stability and complexity in model meta-ecosystems, Nat. Commun. **7**, 12457 (2016).
[46] J. Denk and O. Hallatschek, Self-consistent dispersal puts tight constraints on the spatiotemporal organization of species-rich metacommunities, Proc. Natl. Acad. Sci. USA **119**, e2200390119 (2022).
[47] G. Garcia Lorenzana, A. Altieri, and G. Biroli, Interactions and migration rescuing ecological diversity, PRX Life **2**, 013014 (2024).
[48] NIST digital library of mathematical functions, https://dlmf.nist.gov/8.17.